Vehicle dynamics using a limit surface treatment of the tyre–road interface

S J DiMaggio and **M P Bieniek**
Department of Civil Engineering and Engineering Mechanics, Columbia University, New York, USA

Abstract: A new method of dealing with the force-producing mechanism at the tyre–road interface is presented. The tyre model consists of a representation of the tyre elasticity and the relations between the interface forces and the contact patch displacement. These relations are described in terms of the 'tyre limit surface'. The model appears to be capable of reproducing the tyre behaviour under both free-rolling and fully locked wheel conditions. A satisfactory agreement has been obtained between the available experimental data on the force versus slip parameters and the predictions of the present model. Applications to two problems of vehicle dynamics, oversteer versus understeer behaviour and motion with locked rear wheels, are presented.

Keywords: vehicle dynamics, limit surface treatment, tyre–road interaction, tyre–road interface, force-producing mechanism, computational vehicle dynamics, tyre models, tyre forces, vehicle performance

1 INTRODUCTION

While there has always been a demand for vehicle dynamics simulation, the need for accurate and computationally efficient methods has increased owing to the emergence of new technology such as yaw- and roll-rate sensing and traction control. The optimal interaction between the sensor and the resulting control forces cannot be achieved in an economical manner using trial-and-error experimental techniques, and thus a computational approach must be used. Models have been developed for various applications in the field of vehicle dynamics by a number of researchers. These models vary in their complexity from simple two-degree-of-freedom systems to detailed finite element representations of the entire car. Regardless of the detail used in the formulation of the equations of motion for these models, a comprehensive description of the forces generated at the tyre–road interface is intrinsic to the accuracy of the analysis. In the most general analysis of a vehicle, these forces must be accurate over a wide range of dynamic behaviour, from slow steady-state turning manoeuvres to emergency conditions in which the vehicle is skidding.

Vehicle dynamics models and their applications in analysis, design and driver simulation have been developed by many researchers. The requirements and complexity of these models are largely dependent on their application and this topic has been discussed in depth [**1**, **2**]. The equations of motion governing the vehicle dynamics can be generated using several approaches, from methods in which the analyst derives the equations of motion using only the variables necessary for a particular application [**3**–**5**], to multibody formulations where the system geometry and kinematic quantities and constraints are input to a computer which, in turn, generates the equations of motion [**6**]. Regardless of the approach taken, the success of any vehicle dynamics model depends largely on an accurate determination of the tyre forces.

There are three different approaches to tyre modelling in the context of vehicle dynamics analysis. The first of these uses a physical model of the tyre, as in reference [**7**] where the tyre is made up of discrete deformable radial spokes. Other workers [**8**] use a series of springs which produce forces in the contact patch. A good review of this type of approach has been given in reference [**9**]. Note that the parameters in these models must be set to create a match with measured tyre data. A second approach entails the storage of a large amount of experimental data [**10**], using interpolation to describe arbitrary conditions. The final approach, which appears to be the most popular [**11**–**15**], is to determine a function which relates tyre forces and moments to problem parameters such as slip angle and camber. Through suitable choices of the constants in these empirical relationships, good correspondence to experimental data can be achieved. While some early work could not deal with aggressive vehicle dynamics because simple linear relationships between forces and slip parameters

The MS was received on 23 June 1997 and was accepted for publication on 9 December 1997.

were used, more recent theories can handle a more general class of manoeuvres in which the composite tyre force approaches the friction ellipse. In a complete departure from these traditional approaches, a new method is presented in this paper which uses a mathematically defined limit surface to determine the tyre forces at arbitrary operating conditions.

In order to focus on the new tyre model, the complexity of the automobile dynamics is kept to a minimum. The vehicle is modelled as a rigid body with two translational degrees of freedom in the plane of the ground, which is flat, and one rotational degree of freedom about an axis perpendicular to the ground plane. This approach neglects the effects of roll, pitch and load transfer between the wheels. In the tyre model, self-aligning torques and wheel camber are assumed to be negligible and no time lag in force generation is considered. While various limitations are present owing to this simplified approach, the formulation of the tyre model is kept as general as possible in order that it be compatible with more complex vehicle dynamics which will be considered in the future.

The restrictions imposed by these assumptions are similar to those present in an early paper on the subject [**16**], and the formulation of the vehicle dynamics is therefore comparable. Equations of motion are written in terms of the kinematic variables and the forces and moments acting on the vehicle. After solving these equations and updating the variables and system geometry, new tyre forces are computed. Unlike the formulations in references [**3**] and [**16**], and some other simple vehicle dynamics models, the forces due to the independent left and right wheels are not added to produce a single force at a particular axle. In other words, the yawing moments due to tyre forces parallel to the vehicle centre-line are not neglected.

2 VEHICLE DYNAMICS

The geometry, kinematic variables and forces acting on the vehicle are shown in Fig. 1.

2.1 Kinematics

Two reference frames are necessary in the formulation of vehicle dynamics in this paper. A frame S is fixed in space and described by a unit triad $\boldsymbol{e}_r$, $\boldsymbol{e}_s$, $\boldsymbol{e}_t$, while a unit triad $\boldsymbol{e}_x$, $\boldsymbol{e}_y$, $\boldsymbol{e}_z$, fixed in the vehicle frame V, describes the orientation of the car relative to S. Owing to the simplifications mentioned previously, the unit vectors $\boldsymbol{e}_t$ and $\boldsymbol{e}_z$ are identical and perpendicular to the plane of the road at all times. Therefore, only the unit vector $\boldsymbol{e}_z$ will be used to refer to this direction. In future work, which will include the pitch and roll motions of the vehicle, the independence of these vectors must be maintained.

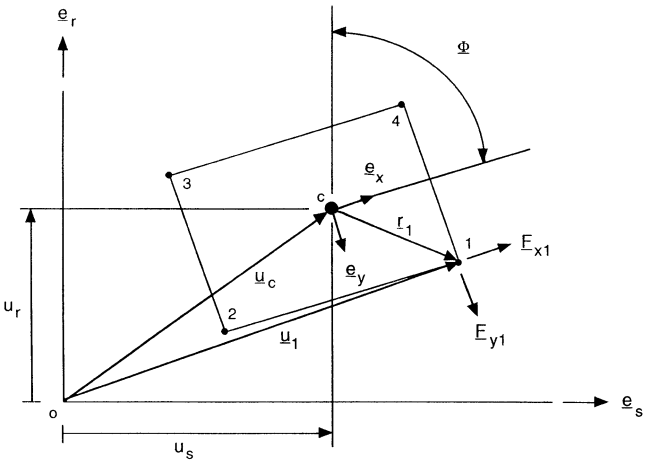

Fig. 1 Vehicle kinematics

Three kinematic variables describe the position and orientation of the vehicle. These are the components of the position vector of the centre of mass:

$$\boldsymbol{u}_c = u_{rc}\boldsymbol{e}_r + u_{sc}\boldsymbol{e}_s \tag{1}$$

and the rotation

$$\boldsymbol{\phi} = \phi \boldsymbol{e}_z \tag{2}$$

of the vehicle frame about an axis through its centre of mass and perpendicular to the ground plane.

The other kinematic quantities of interest will be the position vectors associated with the wheel hubs and the centres of the contact patches. These vectors will not be the same, as it is the relative displacements of the two which leads to the forces in the tyre model to be described in depth later. The position vectors of the wheel hubs are

$$\boldsymbol{u}_i = u_{ri}\boldsymbol{e}_r + u_{si}\boldsymbol{e}_s \tag{3}$$

or

$$\boldsymbol{u}_i = u_{xi}\boldsymbol{e}_x + u_{yi}\boldsymbol{e}_y \tag{4}$$

and the position vectors of the centre of the wheel contact patches are

$$\boldsymbol{d}_i = d_{ri}\boldsymbol{e}_r + d_{si}\boldsymbol{e}_s \tag{5}$$

or

$$\boldsymbol{d}_i = d_{xi}\boldsymbol{e}_x + d_{yi}\boldsymbol{e}_y \tag{6}$$

The subscript $i = 1, 2, 3, 4$ describes the wheels starting from the front right and going clockwise to the front left. This convention and the use of the subscript i will be maintained throughout the rest of this paper. Note that the position vectors of the centres of the contact patches are

not shown in Fig. 1 and only the position vector of one of the wheel hubs is presented.

The position vectors of the wheel hubs are not independent of the position vector and rotation of the vehicle centre of mass. They are related through the equation

$$\boldsymbol{u}_i = \boldsymbol{u}_c + \boldsymbol{r}_i \tag{7}$$

where

$$\boldsymbol{r}_i = r_{xi}\boldsymbol{e}_x + r_{yi}\boldsymbol{e}_y \tag{8}$$

is the position vector of wheel hub i relative to the centre of mass and whose components r_{xi} and r_{yi} are constants.

All the vectors in this work can be written with respect to unit vectors fixed in either of the two frames. The subscripts r and s will denote components with respect to the Newtonian reference frame, while subscripts x and y will indicate components with respect to the vehicle frame. Henceforth, vectors will be presented with components relative to one particular unit triad, with the understanding that the components relative to the other triad can be obtained using a simple coordinate transformation.

2.2 Forces and moments

The forces and moments acting on the vehicle in this paper are due primarily to the forces generated at the tyres. Any additional forces acting on the centre of mass will consist of components P_r and P_s. The forces in the r and s directions are

$$\overline{F}_r = P_r + \sum_i F_{ri} \tag{9}$$

and

$$\overline{F}_s = P_s + \sum_i F_{si} \tag{10}$$

where F_{ri} and F_{si} are the components of the force exerted by the road on the tyre for wheel i and the sums are taken over the number of tyres. Note that in Fig. 1 the components of the tyre force vector for tyre 1 are shown with respect to unit vectors fixed in the vehicle.

The moment acting at the centre of mass about an axis perpendicular to the ground plane is

$$\overline{G} = T + \sum_i G_i \tag{11}$$

where the tyre forces contribute

$$G_i = r_{xi}F_{yi} - r_{yi}F_{xi} \tag{12}$$

and the summation is again over the number of wheels. Any torque not due to the tyre forces is contained in term T.

2.3 Equations of motion

Once the forces are obtained, three second-order ordinary differential equations governing the system are easily obtained. Using equations (9) to (12), these are

$$M\ddot{u}_{rc} = \overline{F}_r = P_r + \sum_i F_{ri} \tag{13}$$

$$M\ddot{u}_{sc} = \overline{F}_s = P_s + \sum_i F_{si} \tag{14}$$

$$I\ddot{\phi} = \overline{G} = T + \sum_i G_i = T + \sum_i (r_{xi}F_{yi} - r_{yi}F_{xi}) \tag{15}$$

In equations (13) to (15) the double dot over a symbol denotes differentiation twice with respect to time in the Newtonian frame, and M and I denote the mass and polar mass moment of inertia respectively relative to the mass centre of the vehicle.

3 THE TYRE MODEL

The tyre model proposed in this paper consists of two components. One of these is the set of elastic springs which models the deformation of the tyre with respect to the wheel hub. The other component is the tyre–road interface which defines the resistance to the rolling or sliding motion of the tyre. The contact between the road and the tyre occurs over a finite area called the contact patch. In this formulation, the contact patch is represented by a point and it is assumed that the forces at the tyre–road interface act at this location.

3.1 Physical representation

A schematic representation of the tyre is shown in Fig. 2. The vector $\boldsymbol{u}_i$ represents the position of the ith reference point on the vehicle frame. Owing to the present assumption of a rigid connection between the wheel hub and the frame, this reference point is also the position of the wheel hub. Thus, in Fig. 2, H_i is the ith wheel hub and P_i is the location of the ith contact patch. The distinction between a reference point and the wheel hub is made so that a more accurate representation of the actual connection between the wheel hub and the frame can be included in future models. The position of the contact patch is represented by the vector $\boldsymbol{d}_i$. Since the wheel plane is not, in general, parallel to the vehicle longitudinal axis $\boldsymbol{e}_x$, an additional coordinate system, defined by unit vectors $\boldsymbol{e}_{\xi i}$ and $\boldsymbol{e}_{\eta i}$, is introduced. Because the wheel camber is not considered, the third unit vector in this triad is $\boldsymbol{e}_z$. In this coordinate

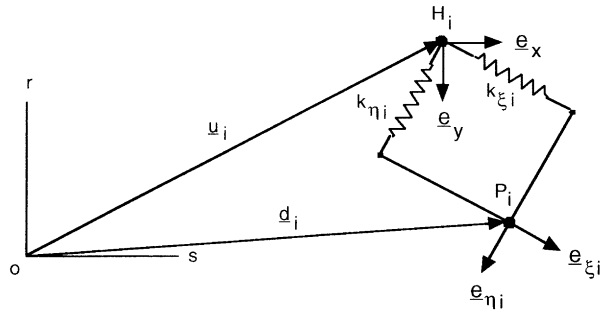

Fig. 2 Tyre model

system, the ξ_i axis remains parallel to the wheel plane at all times. Hence, the displacement of the contact patch relative to the wheel hub is

$$\boldsymbol{d}_i - \boldsymbol{u}_i = (d_{xi} - u_{xi})\boldsymbol{e}_x + (d_{yi} - u_{yi})\boldsymbol{e}_y \tag{16}$$

or

$$\boldsymbol{d}_i - \boldsymbol{u}_i = (d_{\xi i} - u_{\xi i})\boldsymbol{e}_{\xi i} + (d_{\eta i} - u_{\eta i})\boldsymbol{e}_{\eta i} \tag{17}$$

The elasticity of the tyre is represented by the springs $k_{\xi i}$ and $k_{\eta i}$. In general, these springs should be non-linear, consistent with the deformation characteristics of the tyre. The hysteretic properties of the tyre should also be included by introducing some viscoelastic elements. However, in order to simplify the present analysis, the springs are assumed to be linear and the hysteresis is neglected. Accordingly, the force transmitted from the contact patch to the vehicle is related to the relative displacement in equation (17) by

$$\begin{Bmatrix} F_{\xi i} \\ F_{\eta i} \end{Bmatrix} = \begin{bmatrix} k_{\xi i} & 0 \\ 0 & k_{\eta i} \end{bmatrix} \begin{Bmatrix} d_{\xi i} - u_{\xi i} \\ d_{\eta i} - u_{\eta i} \end{Bmatrix} \tag{18}$$

or, using a more compact notation,

$$\boldsymbol{F}_i = \mathbf{K}_i(\boldsymbol{d}_i - \boldsymbol{u}_i) \tag{19}$$

In equation (19), the force vector and the relative displacement vector are referred to the tyre coordinate system ξ_i and η_i. Thus, an additional transformation of the force components from the tyre coordinate system to the global system, s and r, must be performed prior to the substitution of these components into the equations of motion.

3.2 The limit surface

The concept of a limit surface is the main element of the tyre model and the central point of this paper. Specifically, the tyre model is based on the premise that the interaction between a pneumatic tyre and the road can be described by a mathematically defined limit surface. In order to simplify the notation in this section, the subscript i will be dropped.

In general, the forces acting at the tyre–road interface have three components, F_ξ, F_η and F_z, with F_z being normal to the contact patch plane. For the wheel model proposed in this paper, it is postulated that, at any set of vehicle operating conditions, there is a function of the variables F_ξ, F_η, F_z, and, in general, other parameters, such that the equation

$$Y(F_\xi, F_\eta, F_z, \ldots) = 0 \tag{20}$$

defines a surface in the space of forces F_ξ, F_η and F_z, which determines the relation between forces acting on the contact patch and the resulting tyre motion. This tyre motion may consist of rolling, slipping or a combination of the two. In the $F_\xi F_\eta$ plane, equation (20) defines a curve. One function of the surface in equation (20) is to define the maximum magnitude which the interface force can attain at a particular set of operating conditions. In this sense the surface sets a limit on the magnitude of the tyre forces, and thus the term 'limit surface' appears to be appropriate. The form of this limit surface must be determined on the basis of tests for a given tyre and at various sets of road and operating conditions.

As an example, consider an elliptical limit surface defined by

$$\frac{F_\xi^2}{a^2} + \frac{F_\eta^2}{b^2} - 1 = 0 \tag{21}$$

with the parameters a and b depending on F_z and also other variables. By changing the parameters a and b, a narrow ellipse may be obtained for the rolling condition of the wheel, while a fuller ellipse, possibly approaching a circle, can be used for a tyre sliding with a fully locked wheel. Both of these cases are illustrated in Fig. 3.

In addition to setting the maximum magnitude of the interface force, the limit surface must also define the motion of the contact patch. The combination of interface forces such that

$$Y(F_\xi, F_\eta, F_z, \ldots) < 0 \tag{22}$$

corresponds to the contact patch remaining stationary with respect to the road. It is only when $Y(\boldsymbol{F}) = 0$ that the contact patch will move. It is proposed that the direction of tyre motion, which can include both rolling and sliding, is such that the contact patch velocity vector $\dot{\boldsymbol{d}}$ is normal to the limit surface. Note that the dot over $\boldsymbol{d}$ denotes time differentiation in the Newtonian reference frame. Mathematically, this means that

$$(\dot{d}_\xi, \dot{d}_\eta) = \lambda\left(\frac{\partial Y}{\partial F_\xi}, \frac{\partial Y}{\partial F_\eta}\right) \tag{23}$$

or

$$\dot{\boldsymbol{d}} = \lambda \frac{\partial Y}{\partial \boldsymbol{F}} \tag{24}$$

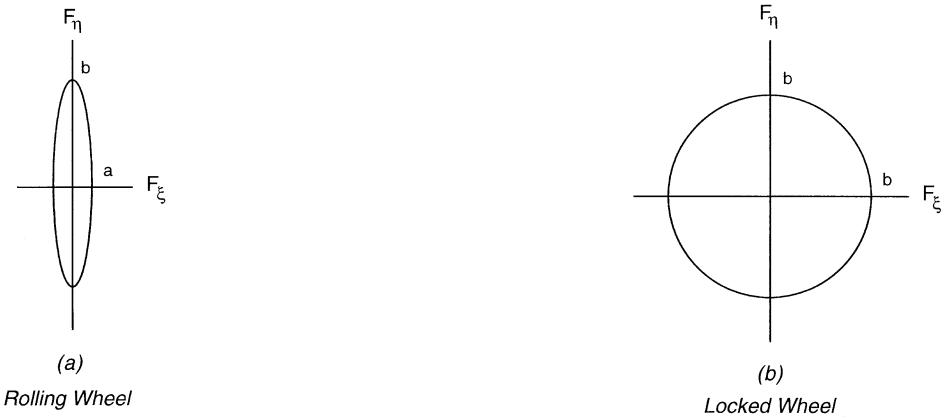

Fig. 3 Examples of the limit surface

where λ is a proportionality factor. The direction of $\dot{\boldsymbol{d}}$ is shown in Fig. 4. Note that by using equations (19) and (24) both the tyre–road interface forces and the contact patch velocity are defined. Equation (19) can also be rewritten in the rate form as

$$\dot{\boldsymbol{F}} = \mathbf{K}(\dot{\boldsymbol{d}} - \dot{\boldsymbol{u}}) \tag{25}$$

Additionally, during the contact patch motion defined by equation (24), the equation of the limit surface in equation (20) must also be satisfied. This equation may also be written in the rate form as

$$\dot{Y} \equiv \frac{\partial Y}{\partial F_\xi}\dot{F}_\xi + \frac{\partial Y}{\partial F_\eta}\dot{F}_\eta \equiv \left(\frac{\partial Y}{\partial \boldsymbol{F}}\right)^{\mathrm{T}} \dot{\boldsymbol{F}} = 0 \tag{26}$$

and, in this form, is referred to as the consistency condition. Combining equations (24), (25) and (26), the parameter λ can be determined:

$$\lambda = \frac{(\partial Y/\partial \boldsymbol{F})^{\mathrm{T}}\mathbf{K}\dot{\boldsymbol{u}}}{(\partial Y/\partial \boldsymbol{F})^{\mathrm{T}}\mathbf{K}(\partial Y/\partial \boldsymbol{F})} \tag{27}$$

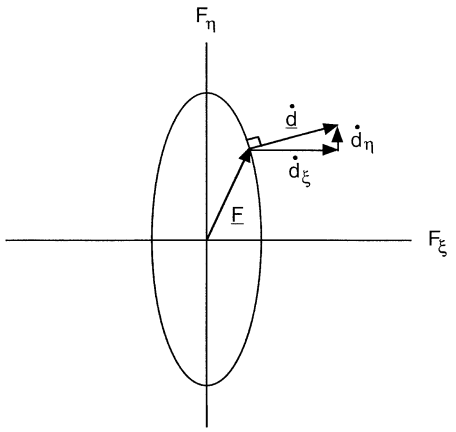

Fig. 4 Direction of the contact patch velocity

Once λ is determined, the motion of the contact patch and the change in the tyre forces can be found using equations (24) and (25).

By inserting the expression for λ into equation (24) and then substituting this into equation (25), the following direct rate relation between the tyre force and the hub displacement is obtained:

$$\dot{\boldsymbol{F}} = \mathbf{D}\dot{\boldsymbol{u}} \tag{28}$$

where

$$\mathbf{D} \equiv \mathbf{K}\left(\frac{(\partial Y/\partial \boldsymbol{F})[(\partial Y/\partial \boldsymbol{F})^{\mathrm{T}}\mathbf{K}]}{(\partial Y/\partial \boldsymbol{F})^{\mathrm{T}}\mathbf{K}(\partial Y/\partial \boldsymbol{F})} - 1\right) \tag{29}$$

is the equivalent tyre stiffness, which includes the effect of the contact patch motion.

4 COMPUTATIONAL IMPLEMENTATION OF THE TYRE MODEL

In order for this method of interface force calculation to be useful, an efficient computational procedure must be available to solve the governing equations of the previous section. These equations are reproduced in their incremental form and a basic solution procedure is presented. Again, the subscript i is supressed.

4.1 Incremental form of the governing equations

The complete set of equations for the calculation of the interface forces consists of the following:

1. The equation of the current limit surface is

$$Y(\boldsymbol{F}, \ldots) = 0 \tag{30}$$

2. The sliding rule is:

(a) If $Y = 0$ and $(\partial Y/\partial \boldsymbol{F})\,\dot{\boldsymbol{F}} > 0$,

$$\Delta \boldsymbol{d} = \Delta\lambda \frac{\partial Y}{\partial \boldsymbol{F}} \tag{31}$$

(b) If $Y < 0$ or $(\partial Y/\partial \boldsymbol{F})\dot{\boldsymbol{F}} < 0$,

$$\Delta \boldsymbol{d} = 0 \tag{32}$$

3. The consistency condition is

$$\Delta Y = \frac{\partial Y}{\partial \boldsymbol{F}}\,\Delta \boldsymbol{F} = 0 \tag{33}$$

which holds in case (a) above and which is used to eliminate $\Delta\lambda$ in equation (31).

4. An incremental form of the force–deflection law in equation (25) is

$$\Delta \boldsymbol{F} = \mathbf{K}(\Delta \boldsymbol{d} - \Delta \boldsymbol{u}) \tag{34}$$

This can be rewritten as

$$\Delta \boldsymbol{F} = \Delta \boldsymbol{F}^{\mathrm{N}} + \Delta \boldsymbol{F}^{\mathrm{S}} \tag{35}$$

where

$$\Delta \boldsymbol{F}^{\mathrm{N}} = -\mathbf{K}\,\Delta \boldsymbol{u} \tag{36}$$

and

$$\Delta \boldsymbol{F}^{\mathrm{S}} = \mathbf{K}\,\Delta \boldsymbol{d} \tag{37}$$

4.2 Return algorithm

Once the equations of motion (13) to (15) are solved, the incremental hub displacement $\Delta \boldsymbol{u}$ is known owing to the treatment of the vehicle as a rigid body. During one time step, let $\Delta \boldsymbol{F}$ be the total increment in the interface force from an initial force $\boldsymbol{F}_0$ to a final force $\boldsymbol{F}_2$:

$$\boldsymbol{F}_2 = \boldsymbol{F}_0 + \Delta \boldsymbol{F} \tag{38}$$

The steps needed to calculate $\boldsymbol{F}_2$ are referred to as the return algorithm and are as follows:

1. Use the value of $\Delta \boldsymbol{u}$ to obtain the first part of the increment in force $\Delta \boldsymbol{F}$:

$$\Delta \boldsymbol{F}^{\mathrm{N}} = -\mathbf{K}\,\Delta \boldsymbol{u} \tag{39}$$

2. Add $\Delta \boldsymbol{F}^{\mathrm{N}}$ to the initial force $\boldsymbol{F}_0$ to obtain $\boldsymbol{F}_1$:

$$\boldsymbol{F}_1 = \boldsymbol{F}_0 + \Delta \boldsymbol{F}^{\mathrm{N}} \tag{40}$$

At this point, if the force vector $\boldsymbol{F}_1$ lies inside the limit surface, the total increment in force is $\Delta \boldsymbol{F} = \Delta \boldsymbol{F}^{\mathrm{N}}$ and no motion of the contact patch develops. However, consider a force vector $\boldsymbol{F}_1$ which lies outside the limit surface $Y(\boldsymbol{F}) = 0$:

$$Y(\boldsymbol{F}_1) = c \tag{41}$$

where $c > 0$.

3. One must therefore 'return' to the limit surface. This means that the final force vector $\boldsymbol{F}_2$ must be determined. This vector must satisfy the condition that $Y(\boldsymbol{F}_2) = 0$. From Fig. 5 and equation (35), it can be seen that $\Delta \boldsymbol{F}^{\mathrm{S}}$ is the vector which will return the force to the limit surface.

4. Approximately (using a discrete form of the consistency condition between $\boldsymbol{F}_1$ and $\boldsymbol{F}_2$),

$$Y(\boldsymbol{F}_2) - Y(\boldsymbol{F}_1) = \frac{\partial Y}{\partial \boldsymbol{F}} \cdot \Delta \boldsymbol{F}^{\mathrm{S}} \tag{42}$$

or

$$-Y(\boldsymbol{F}_1) = \frac{\partial Y}{\partial \boldsymbol{F}} \cdot \Delta \boldsymbol{F}^{\mathrm{S}} \tag{43}$$

5. Combining equations (31), (37) and (43),

$$\Delta\lambda = \frac{-Y(\boldsymbol{F}_1)}{(\partial Y/\partial \boldsymbol{F})^{\mathrm{T}}\mathbf{K}(\partial Y/\partial \boldsymbol{F})} \tag{44}$$

The incremental force $\Delta \boldsymbol{F}$, and therefore the final force $\boldsymbol{F}_2$, follow immediately from equations (31), (35) and (37).

The above scheme yields only an approximate value of the final force $\boldsymbol{F}_2$ at the end of a time step. The errors stem from the use of finite increments of the displacements and forces in the simple first-order formulae and the calculation of the limit surface gradients at the point $\boldsymbol{F}_1$, which does not determine the exact direction of the contact patch displacement increment. The magnitude of the errors can be reduced by decreasing the time step of the numerical integration of the equations of motion at the expense,

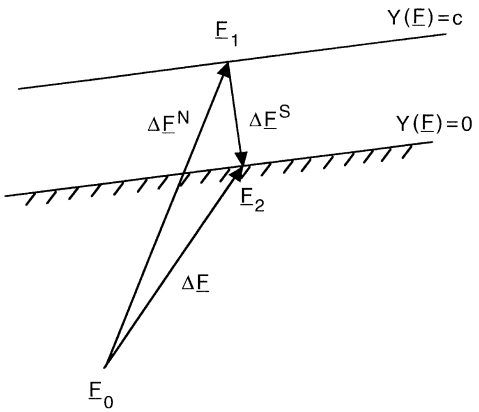

Fig. 5 Return to the limit surface

however, of the computational efficiency of the procedure. In the examples given in this paper, subcycling of the return algorithm within a given time step and certain iteration procedures have been explored. Progress on the optimal methods of improving the accuracy of the calculations will be reported shortly.

5 APPLICATIONS

5.1 Example 1: force versus slip angle carpet plot

For the method proposed to be useful, it must be able to represent real tyre lateral force data. To show that this can be done with the tyre model proposed in this paper, lateral force versus slip angle and normal force results are compared with those given by Nordeen and Cortese [**18**]. The data are given for three values of normal force between 600 and 1400 lbf.

The elliptical limit surface shown in Fig. 3a is used to model a rolling tyre. The direction of contact patch motion, by virtue of equation (24), is normal to the limit surface and shown in Fig. 4. Therefore, what is commonly referred to as the slip angle α is actually the angle formed by the normal to the limit surface and the ξ axis. Since the equation for the limit surface is

$$Y \equiv \frac{F_\xi^2}{a^2} + \frac{F_\eta^2}{b^2} - 1 = 0 \tag{45}$$

the equation relating lateral force and slip angle is

$$\alpha = \arctan\left(\frac{(\partial Y/\partial \boldsymbol{F}) \cdot \boldsymbol{e}_\eta}{(\partial Y/\partial \boldsymbol{F}) \cdot \boldsymbol{e}_\xi}\right) = \arctan\left(\frac{a^2 F_\eta}{b^2\sqrt{\left[a^2\left(1 - \dfrac{F_\eta^2}{b^2}\right)\right]}}\right) \tag{46}$$

The η intercept on the limit surface is equal to the normal force N times the coefficient of friction μ at the tyre–road interface. This coefficient is a function of the normal force on the tyre and is chosen such that there is good correlation with experimental force–slip angle measurements at the largest slip angles [**8**]. The ξ intercept is then chosen to ensure that the lateral force at small slip angles is linear and not a function of the normal force [**18**]. In this manner, using an extremely simple curve-fitting technique, the following relations for the ξ and η intercepts on the limit surface of Fig. 3a were generated (in SI units):

$$a = \frac{b^2}{50\,939.25} \tag{47}$$

and

$$b = \mu(N)N \tag{48}$$

where

$$\mu(N) = 1.16 - 5.12 \times 10^{-4} N + 2.03 \times 10^{-7} N^2 \tag{49}$$

A comparison of the present results with the data in reference [**18**] is given in Fig. 6. Small discrepancies can be attributed to the fact that the curve fitting was done with data points scaled from the original figure given in reference [**18**]. Using the exact numerical data and a more rigorous curve-fitting procedure would lead to a better fit between the two sets of results.

5.2 Example 2: Olley's oversteer–understeer problem

Another of the requirements for the tyre model should be its ability to treat the directional control properties of a vehicle. One example which can be used to verify this ability was introduced by Olley [**19**], and later discussed in references [**20**, **21**], among others. In Olley's problem, a lateral force is applied to the centre of gravity of a vehicle which is moving in a straight line with no steer angle. It can be shown that an oversteer vehicle follows a trajectory which curves towards the input force. The understeer vehicle follows a trajectory which curves away from the force, while the neutral steer vehicle deviates away from the input in a straight line.

In this example, the understeer, neutral steer and oversteer vehicles are characterized by having their engines in the front, centre and rear of the vehicle respectively. The tyre properties for all four rolling wheels are the same as those given in Example 1.

The geometry of the vehicle used in this example is shown in Fig. 7, where the shaded area indicates the engine location. The three vehicles examined have their engines positioned with the centres of mass at $r_E = -1.05$, 0.0 and 1.05 m for the oversteer, neutral steer and understeer cases respectively. The total vehicle mass is 570 kg, the engine mass is 150 kg, and both are assumed uniform over their respective areas. The initial velocity of the vehicle is 10 m/s and a lateral Heaviside step input force of magnitude $P_0 = 600$ N is applied.

The trajectories for the three cases are consistent with previous results and are shown in Fig. 8 for displacements in the r direction up to 60 m.

5.3 Example 3: stability of vehicles with locked rear wheels

In this example a straight-moving rolling vehicle is subjected to a small angular disturbance, in the form of a small angular velocity input ω_0, at the same time that the two rear wheels are locked. No front steer angles are input to the problem. It has been shown by Koiter and Pacejka [**3**], as well as other workers, that this type of input leads to instability of the vehicle as the forward speed increases. In

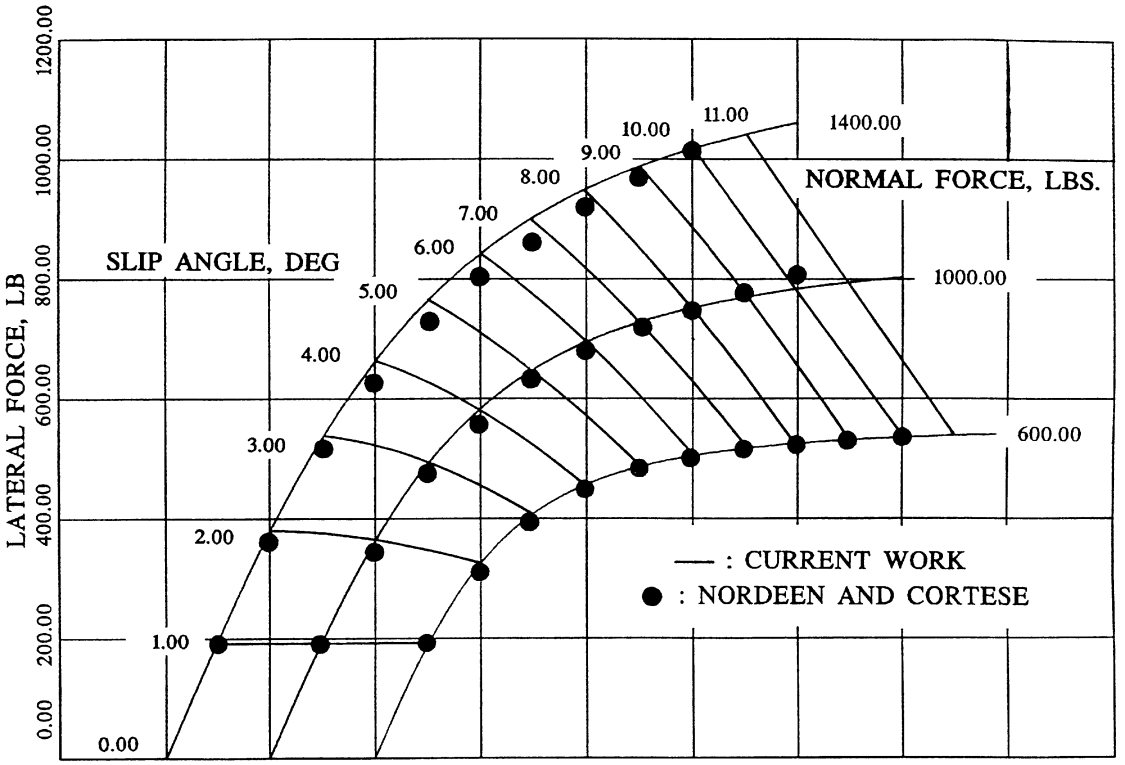

Fig. 6 Lateral force versus slip angle and normal force

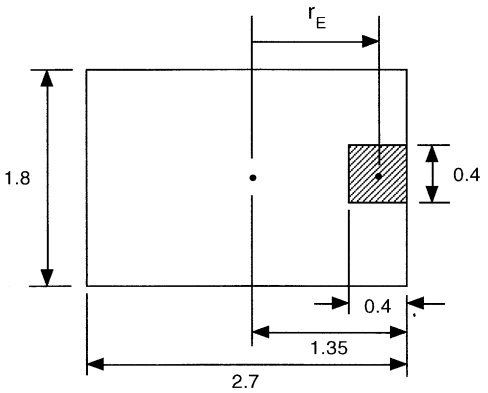

Fig. 7 Vehicle geometry

this example, instability will be characterized by the following equation:

$$\frac{\phi(t_s)}{\hat{\phi}(t_s)} > 1 \tag{50}$$

where

$$\hat{\phi}(t_s) = \omega_0 t_s \tag{51}$$

and t_s is the time that it takes the vehicle to come to rest. Note that ϕ is the angle between the $\boldsymbol{e}_x$ unit vector, which is fixed in the vehicle, and the $\boldsymbol{e}_r$ unit vector, which is fixed in space. For the neutral steer vehicle of Example 2, the initial velocity leading to instability was approximately 10.8 m/s.

Koiter and Pacejka [**3**] gave an estimate for this critical velocity as

$$V_{cr} = \sqrt{(\mu g L)} \tag{52}$$

where L is the distance between front and rear axles. For the geometry in this example this leads to a critical velocity of 4.72 m/s. The large difference in results is mostly attributable to the fact that Koiter and Pacejka [**3**] modelled the rolling wheels at the front as a pair of skates. They did state that the critical speed is increased by about 10 per cent by the introduction of a finite cornering stiffness for the front wheels. Furthermore, the critical speed given by equation (52) was developed from equations which assumed that the rotation of the vehicle about an axis perpendicular to the road surface was small and yawing moments due to tyre forces parallel to the vehicle centreline were not considered. The definition of instability in reference [**3**] is that the initial disturbed angular velocity increases in the ensuing motion. This is obviously not the same as the definition in equation (50), which expresses the condition that the initial disturbance is amplified at the time when the vehicle stops. The comparison of the results in this example with those in reference [**3**], therefore, is useful only in the qualitative sense.

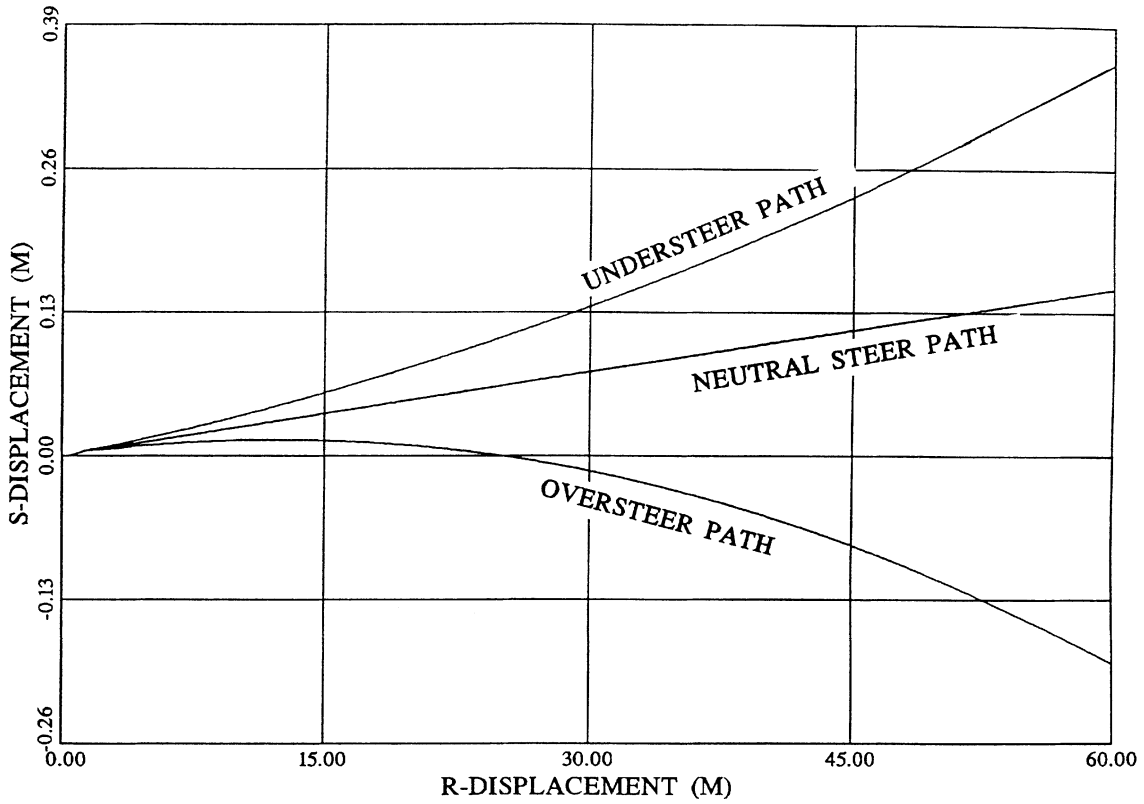

Fig. 8 Olley's oversteer–understeer problem

To model the locked rear wheels, the circular limit surface shown in Fig. 3b was used. The ξ and η intercepts b are taken from equations (48) and (49) in Example 1. Note that with a circular limit surface the direction of the contact patch motion is parallel to the direction of the frictional force. This is consistent with the assumption of many workers when considering the frictional force produced by the skidding of a locked wheel across the road surface.

In this example, the assumption is that the limit surface changes instantaneously from a rolling (elliptical) to a fully locked (circular) limit surface. More refined models will use a braking slip parameter to change the ξ intercept of the limit surface from its rolling shape to its fully locked shape in a continuous manner.

6 CONCLUDING REMARKS

As the complexity of automotive control systems increases, the need for accurate computer modelling of the vehicle becomes imperative. Without these models, calibration of the control systems for use with input data obtained from sensors in the car becomes prohibitively expensive. Furthermore, because the purpose of these systems is to help to control automobiles during extreme handling manoeuvres while remaining active during normal driving circumstances, the vehicle models must be dependable at all operating conditions.

The tyre model presented in this paper is aimed at representing the tyre elasticity as well as the displacement of the tyre–road contact patch and the forces transmitted from the road to the vehicle. The concept of the limit surface has been shown to be capable of reproducing the longitudinal and transverse tyre behaviour under free-rolling and fully locked wheel conditions. The model requires experimental determination of a relatively small number of parameters and is computationally efficient, even at the present stage of a low degree of optimization of the computational procedures. Additionally, it can be used together with vehicle models of considerably higher complexity than those employed in this paper.

Immediate consideration is being given to the computational efficiency of the return algorithm. Once this is done, the effects of braking and longitudinal slip will be considered. For instance, as mentioned in Example 3, the braking phenomenon will be modelled by allowing the ξ-axis intercept of the limit surface to change from its rolling (elliptic) value to its fully locked (circular) value in a continuous manner. This change in the intercept will be some function of the longitudinal slip. Finally, the complexity of the vehicle dynamics will be increased to include pitch and roll motions of the car and the tyre model will be expected to incorporate the effects of such phenomena as wheel camber, self-aligning torques and time lag in force generation.

REFERENCES

1 **Allen, R. W.** and **Rosenthal, T. J.** Requirements for vehicle simulation models. SAE paper 940175, 1994.

2 **Suresh, B. A.** and **Gilmore, B. J.** Vehicle model complexity: how much is too much? SAE paper 940656, 1994.

3 **Koiter, W. T.** and **Pacejka, H. B.** Skidding of vehicles due to locked wheels. *Proc. Instn Mech. Engrs*, 1968–9, **183**(3H).

4 **Segel, L.** Theoretical prediction and experimental substantiation of the response of the automobile to steering control. *Proc. Instn Mech. Engrs*, 1956.

5 **Whitcomb, D. W.** and **Milliken Jr, W. F.** Design implications of a general theory of automobile stability and control. *Proc. Instn Mech. Engrs*, 1956.

6 **Lieh, J.** A multibody dynamics program for truck simulation. SAE paper 942303, 1994.

7 **Sharp, R. S.** and **El-Nashar, M. A.** A generally applicable digital computer based mathematical model for the generation of shear forces by pneumatic tyres. *Vehicle Syst. Dynamics*, 1986, **15**, 187–209.

8 **Bernard, J. E., Segel, L.** and **Wild, R. E.** Tire shear force generation during combined steering and braking maneuvers. SAE paper 770852, 1977.

9 **Pacejka, H. B.** Analysis of tire properties. In *Mechanics of Pneumatic Tires* (Ed. S. K. Clark), 2nd edition, NBS Monograph 122, 1981, Ch. 9 (National Bureau of Standards, Washington, D.C.).

10 **Flegl, H., Foldi, Th.** and **Witte, L.** Handling characteristics of four-wheel drive vehicles. In Proceedings of the Eighth Symposium on *The Dynamics of Vehicles on Roads and on Railway Tracks* (Eds Lisse, Swets and Zeitlinger), 1984, pp. 165–178.

11 **Pacejka, H. B.** and **Bakker, E.** The magic formula tyre model. In Proceedings of the First International Colloquium on *Tire Models for Vehicle Dynamics Analysis*, Delft, The Netherlands, 21–22 October 1991, pp. 1–18.

12 **Segel, L.** The tire as a vehicle component. In *Mechanics of Transportation Suspension Systems*, The Winter Meeting of the ASME, Houston, Texas, 30 November–5 December 1975 (American Society of Mechanical Engineers, New York).

13 **Lugner, P., Lorenz, R.** and **Schindler, E.** The connexion of theoretical simulation and experiments in passenger car dynamics. In Proceedings of the Eighth IAVSD Symposium on *The Dynamics of Vehicles on Roads and on Railway Tracks* (Eds Lisse, Swets and Zeitlinger), 1984, pp. 317–330.

14 **Heydinger, G. J.** Improved simulation and validation of road vehicle handling dynamics. PhD dissertation, The Ohio State University, Columbus, Ohio, 1990.

15 **Allen, R. W., Magdaleno, R. E., Rosenthal, T. J., Klyde, D. H.** and **Hogue, J. R.** Tire modeling requirements for vehicle dynamics simulation. SAE paper 950312 (SP-1074), 1995.

16 **Radt, H. S.** and **Milliken, W. F.** Motions of skidding automobiles. SAE paper 600133 (205A), 1960.

17 **Bieniek, M. P., Kutt, L. M.** and **Piaszczyk, C. M.** Some problems of analysis of nonlinear elasto-plastic structures. In Proceedings of the NUMETA '85 Conference, Swansea, 7–11 January 1985.

18 **Nordeen, D. L.** and **Cortese, A. D.** Force and moment characteristics of rolling tires. SAE paper 640028 (713A), 1964.

19 **Olley, M.** National influences on American passenger car design. *Proc. Instn Auto. Engrs*, 1937–8, **32**.

20 **Bundorf, R. T.** and **Leffert, R. L.** The cornering compliance concept for description of vehicle directional control properties. SAE paper 760713, 1976.

21 **van Eldik Thieme, H. C. A.** Cornering and camber experiments. In *Mechanics of Pneumatic Tires* (Ed. S. K. Clark), 2nd edition, NBS Monograph 122, 1981, Ch. 8.3 (National Bureau of Standards, Washington, D.C.).